Available online at www.sciencedirect.com
SCIENCE DIRECT®
Diamond and Related Materials 12 (2003) 1315–1321
DIAMOND AND RELATED MATERIALS
www.elsevier.com/locate/diamond

Optical and surface analysis of DC-reactive sputtered AlN films

A. Mahmood[a], R. Machorro[a,*], S. Muhl[b], J. Heiras[a], F.F. Castillón[a], M.H. Farías[a], E. Andrade[c]

[a]*Centro de Ciencias de la Materia Condensada, UNAM, Apdo. Postal 2681, Ensenada, B.C. 22800, Mexico*
[b]*Instituto de Investigacion en Materiales, Circuito esterior s/n CU 70-360, Coyoacan 04510, Mexico DF*
[c]*Instituto de Física, UNAM, Apdo. Postal 20-364, Mexico, D.F. CP 01000, Mexico*

Received 10 April 2002; received in revised form 21 January 2003; accepted 27 January 2003

Abstract

A set of aluminium nitride (AlN), thin films were prepared by DC-reactive magnetron sputtering. The deposition parameters, such as substrate temperature, sputtering gas composition and plasma current were varied. Spectroscopic ellipsometry, XPS, RBS, XRD, SEM, AFM and FTIR techniques were utilized to study the relationship between film properties and preparation conditions. We observed that the optical and surface properties have a strong dependence on the deposition rate. All prepared films present a composition close to AlN stoichiometry, even for nitrogen to argon gas concentrations below 1:2. The near surface of AlN films exposed to atmosphere was primarily composed of Al_2O_3 while the bulk was AlN with some minor contamination of oxygen and carbon. The thickness of the oxide layer was reduced when higher plasma current and lower nitrogen concentration were used. Deposits prepared at 400 °C presented the best refractive index and deposition rate, for both utilized plasma currents.

Keywords: Aluminium nitride, sputtering; Film; Ellipsometry; Oxidation

1. Introduction

Aluminium nitride (AlN) has some outstanding physical properties that have attracted much interest. Hardness, high thermal conductivity, resistance to high temperature and caustic chemicals, combined with a reasonable thermal match to Si and GaAs, are properties that make it an attractive material for electronic packing applications [1]. Its wide band gap has led to investigation of its potential as an insulating material for GaAs and InP based electronic device structures [2]. It also has attractive piezoelectric properties, which are suitable for surface acoustic wave device applications [3]. However, the main interest in AlN comes from the properties of its alloys with GaN, which may permit the fabrication of AlGaN based optical devices active from the blue wavelengths well into the ultraviolet (UV) [4].

AlN thin films have been prepared by a variety of techniques including chemical vapour deposition (CVD) [5], reactive sputtering [6], reactive evaporation [7], molecular beam epitaxy [8,9], ion beam-assisted deposition [10], laser [11] and plasma assisted CVD [12] and metal organic chemical vapour deposition (MOCVD) [13].

Due to the affinity of AlN for oxygen [14], all commercially available AlN material contains a surface oxide layer, which greatly influences the physical properties, such as, the thermal conductivity. This may also cause shifts in luminescence peaks [15], and modify the electronic structure [16]. Furthermore, the difficulty of obtaining and maintaining an oxygen-free AlN surface has complicated many of the experimental studies of the optical properties of this compound. The purpose of this work was to study the surface oxygen content in AlN thin films prepared by the DC reactive magnetron sputtering (DC-RMS), its relation with the optical properties of the deposit and to determine the dependency of these properties with the chemical structure and deposition parameters.

2. Experimental procedure

Pieces of [100] and [111] Si wafers of approximately 1 cm^2 were used as substrates to grow AlN films using DC-RMS in a stainless steel vacuum chamber connected

*Corresponding author. Tel.: +52-646-1744602; fax: +52-646-1744603.
E-mail address: roberto@ccmc.unam.mx (R. Machorro).

0925-9635/03/$ - see front matter © 2003 Elsevier Science B.V. All rights reserved.
doi:10.1016/S0925-9635(03)00076-1

Table 1
The temperature, plasma current and voltage used for the preparation of the different samples

Sample	S(A)	S(B)	S(C)	S(D)	S(E)	S(F)	S(G)	S(H)
T_s (°C)	350	400	450	500	350	400	450	500
I_p (A)	0.45	0.45	0.45	0.45	0.2	0.2	0.2	0.2
V (V)	320	320	320	320	310	310	310	310

to a turbo molecular pump capable of producing a pre-deposition base pressure of 3×10^{-7} Torr. A 4-in. magnetron source was used with a high purity (99.999 at.%) aluminium target. The gas flows were controlled using electronic mass flow meters and the gas pressure was measured using a capacitance vacuum gauge. The substrates were cleaned in $NH_4OH:H_2O_2:H_2O$ and $HCl:H_2O_2:H_2O$ for 5 min each, then rinsed with deionized water. The Al target was sputter cleaned for 5–10 min, before the shutter was opened to start the deposit under the established conditions. Sputtering was carried out in mixed $Ar–N_2$ discharges at different plasma currents; the purity of Ar and N_2 gases was 99.999 wt.%. For the present work the deposition parameters were varied within the following range: working gas pressure $P=4–7$ mTorr, gas composition ratio $N_2/Ar=0.25–4$, substrate temperature $T_s=200–700$ °C and plasma current $I_p=0.2–0.5$ A. However, after the preliminary optimization the gas pressure, N_2/Ar ratio, total gas flow and target to substrate distance were kept fixed at the following values: 6 mTorr, 2/3, 10 sccm and 3 cm. A set of eight samples was selected. These samples were prepared using the values of T_s, I_p and V shown in Table 1.

The complex refractive index as a function of photon energy, obtained using a UVISEL Jobin Yvon ellipsometer, was used to measure the band gap, and the light absorption or transparency. Similarly, a Nicolet model 205 FTIR with a measurement range of 400–4000 cm^{-1} was employed to study the produced films.

For the XPS analysis, a Riber system equipped with a Cameca-Mac3 electron energy analyser was employed using the non-monochromatic Kα radiation line of Mg (1253.6 eV) as the excitation source. The spectra were collected acquiring data every 0.1 eV with an energy resolution of 0.5 eV. The binding energy (BE) of each peak was calibrated by using as a reference the 1s core level of carbon at 284.5 eV. A Philips Diffractometer model X'Pert was employed for the X-ray diffraction (XRD) measurements in order to study the microstructure of the deposits.

The ion beam analysis facilities at the National Autonomous University of Mexico based on a vertical single-end 5.5 MeV Van de Graff accelerator [17] was used to obtain the atomic density (atoms/cm^2) and the elemental composition of the aluminium nitride films. An 1140 keV deuterium beam was used to analyze the AlN films. A solid-state detector (300-mm thick) set at $\theta=165°$ and standard electronics were used to measure the charged particle energy spectra. Quantitative analysis of the particle energy spectra of the deposited films was obtained by using the SIMNRA program [18]. Nuclear reactions with positive 'Q' values $^{14}N(d, a_1)^{12}C^*$, $^{16}O(d, p_1)^{17}O$ and $^{12}C(d, p_0)^{13}C$ were observed as peaks in the high-energy part of the particle energy spectrum almost free of background counts and their counting yield were used to obtain the N, O and C concentration of the films.

3. Results

Before the ellipsometric characterization was performed, we measured a clean Si wafer, to check the instrument setup. The ellipsometric parameters (ψ, Δ) were obtained for all the samples, and some were repeated with greater detail to verify that the small fluctuations were real signals and not noise. Some of the curves of (ψ, Δ) vs. photon energy contain oscillations due to interference effects because the thickness of several samples were of the order of 1 μm. During film growth, the deposition parameters were maintained as constant as possible, but even so some fluctuation may occur, introducing variations in the optical properties of the deposit, as can be seen in the Δ vs. photon energy curves. Our effort was focused on using the simplest multi-layer system as possible to model the films. When a uniform AlN film was assumed, the simulation of the obtained ellipsometric spectra did not provide a good fit between the experimental and theoretical data. However, after fitting using a multi-layer model, i.e., $Al_2O_3/AlN/SiO_2$, a dramatic improvement was obtained. Moreover, when voids were introduced in the second layer, inside the bulk of the material, a further improvement was observed in the fitting. Considering the substrate temperatures of our deposits, the introduction of voids is a plausible option, because we are at the lower end of the Movchan and Demchishin diagram. The granular or columnar growth, inherent in films deposited at low pressure/temperature, necessarily produces voids [19].

We also tried to model a more complex system introducing a mixture of voids, Al and AlN in both upper and central layers, but the results were not consistent, i.e., the mean square error was not reduced. Therefore, we choose a three-layer model; introducing voids in the second layer as shown in Fig. 1, which we

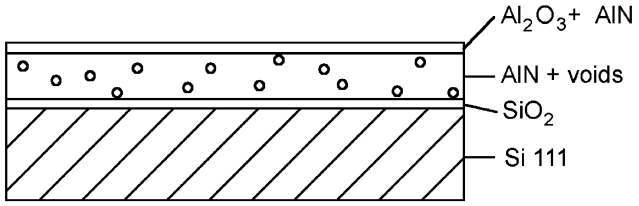

Fig. 1. A schematic of the three-layer model, consisting of homogenous individual layers of $(Al_2O_3+AlN)/(AlN+voids)/SiO_2$ on a substrate of Si(1 1 1), with sharp boundaries and no inter-diffusion or rough interfaces, used in the simulation of the ellipsometric data.

consider, adequately reproduced the film morphology. Fig. 2 shows the simulation of the ellipsometric parameters (ψ, Δ) using the three-layer model that consists of homogenous individual layers of $(Al_2O_3+AlN)/(AlN+voids)/SiO_2$ on a substrate of Si, with sharp boundaries and no inter-diffusion or rough interfaces.

The SiO_2 layer used was the natural silicon oxide (2.4-nm thick) characterized prior the deposition. The starting point for the dispersion curve of AlN is the in situ characterization of a deposition of a 45-nm thin layer. The ellipsometer program adjusts this curve to the best fit to the experimental data. The optical data for the Al_2O_3 were taken from Ref. [20]. The volume fraction and thickness of the layers were varied from sample to sample.

The model for refractive index is expressed by the Lorentz dispersion equation, for a single oscillator, as:

$$\varepsilon(\mathrm{E}) = \varepsilon_\alpha + \mathrm{A}/(\mathrm{E}_\mathrm{f}^2 - \mathrm{E}^2 - \mathrm{iBE})$$

where $E=h\nu$(in eV), $e_\alpha=1.3275$, $A=223.9$, $B=0.029734$ and $E_f=8.574$.

As an example, Fig. 2 shows this process for sample S(B). In general, the agreement was very good when a small percentage of voids in the central layer was introduced.

Fig. 3 demonstrates the variation of complex refractive index vs. photon energy for samples S(A), S(B), S(C), S(D), S(E), S(F) and S(H). The data from Palik [20] has also been included for comparison. Fig. 4 shows the variation of (a) deposition rate vs. temperature and (b) refractive index vs. temperature, for the eight selected films, S(A) through S(H). From this data, it can be noted that there is a direct relationship between the refractive index and the deposition rate. The refractive index of our samples has values in the range 2.1–2.53, considerably higher than other reported values [21–23].

The XRD spectra indicated that films deposited at T_s between 400 and 500 °C, $P=6$ mTorr , plasma power corresponding to 0.45 A, 320 V and $N_2/Ar=40/60$, were crystalline with a [002] preferred orientation, the *c*-axis perpendicular to the substrate surface, as the only peak observed is centered at $2\theta=36.04°$. However, at other deposition conditions a mixture of [002] and [100] preferred orientations, peak centered at $2\theta=33.22°$ and *c*-axis parallel to the substrate surface, was also

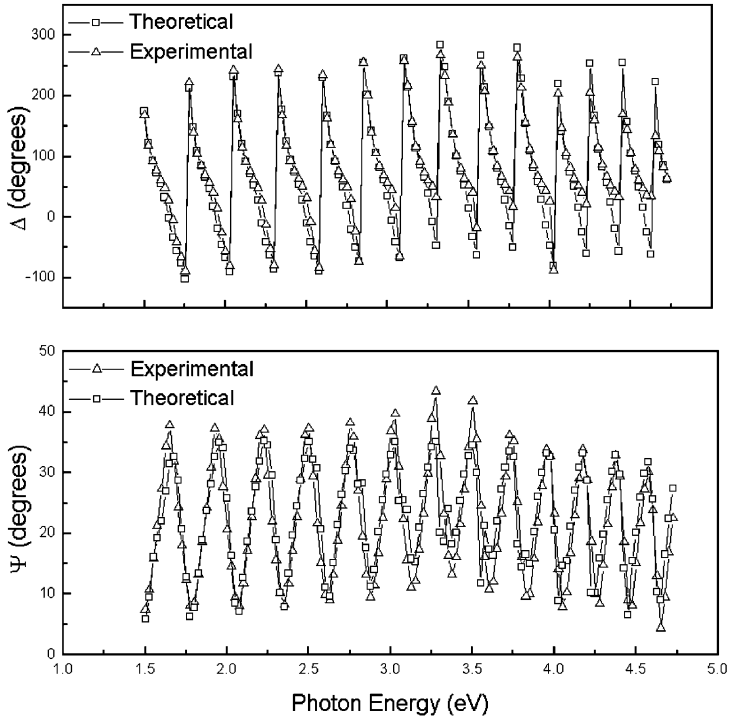

Fig. 2. Typical ellipsometric spectra of sample S(B), together with the simulated curves.

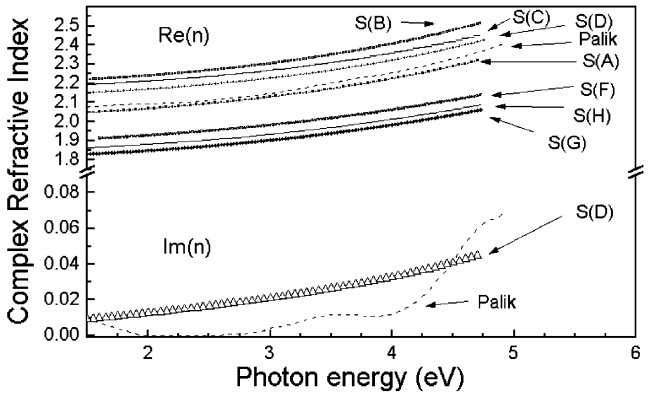

Fig. 3. The variation of complex refractive index vs. photon energy for samples S(A), S(B), S(C), S(D), S(E), S(F) and S(H). The data from Palik has been also included for comparison.

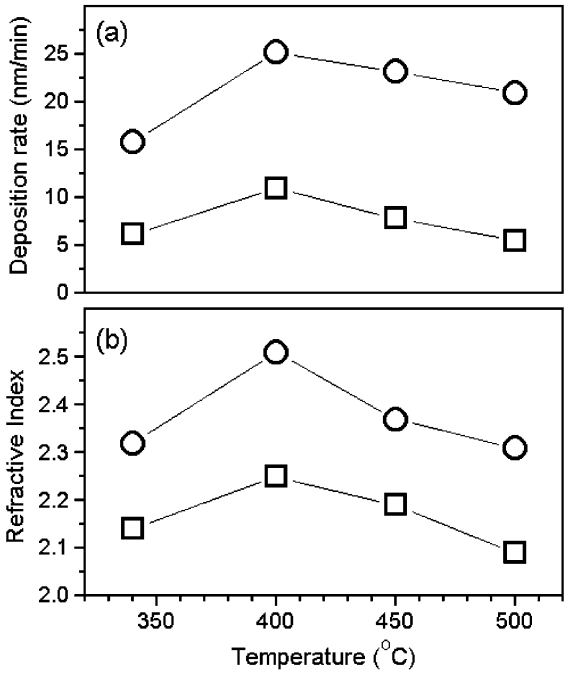

Fig. 4. The variation observed in the reported films of (a) deposition rate vs. temperature and (b) refractive index vs. temperature.

observed. The relative intensity of the (1 0 0) peak to the (0 0 2) peak increased drastically for higher N_2/Ar concentrations.

Fig. 5 shows a typical FTIR spectrum of the AlN films and demonstrates that the fundamental absorption of AlN for the samples occurs at approximately 675 cm^{-1}.

The ion beam elemental analysis was carried out on all of the prepared films and the spectrum was simulated assuming a film 6.5×10^{18} atoms/cm^2 thick with the following elemental composition: $Al_{0.46}N_{0.45}O_{0.06}C_{0.03}$. This analysis shows that the films have, within the experimental error, an Al/N ratio of 1:1. The oxygen in the films is probably due to the oxidation of the AlN films. Part of the carbon concentration may also be due to atmospheric contamination.

The chemical structure of the films was determined by measuring the core level spectra of Al $2p_{3/2}$, N 1s,

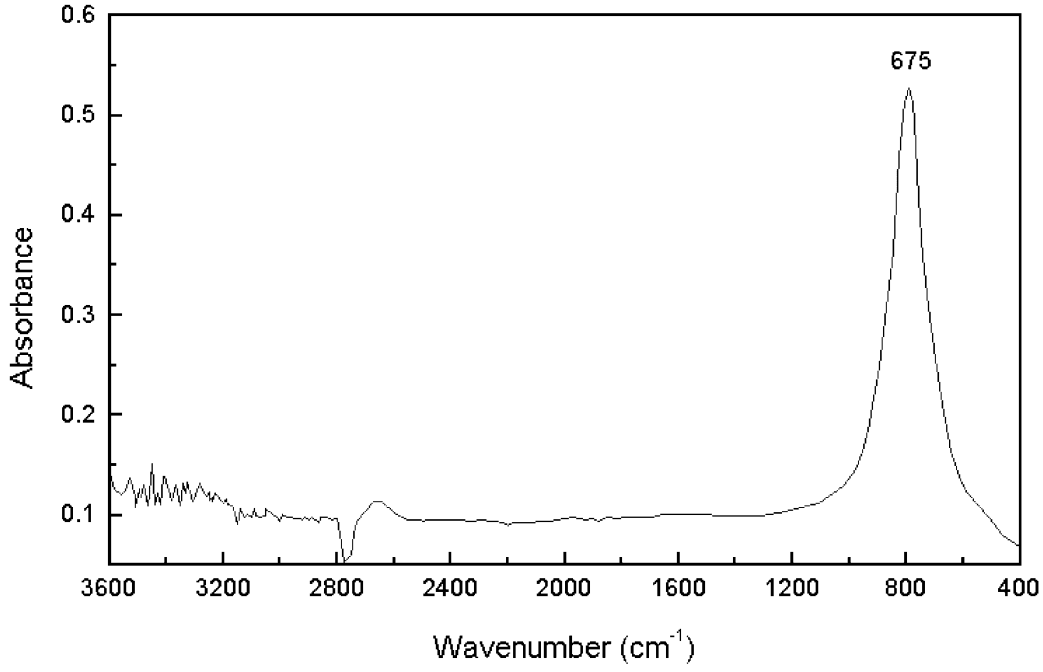

Fig. 5. A typical FTIR spectrum of the AlN films.

C 1s and O 1s. To observe the effect of the chemical bonding nature on the surface, the samples were heated to 200 °C under a vacuum of 10^{-8} Torr. Samples were analyzed by XPS before and after heat treatment. The obtained spectra were deconvoluted and the BE of each core level, for Al $2p_{3/2}$ and N 1s transitions of sample S(B), are presented in Table 2. This table also presents the results of a least square fit analysis of the peaks, i.e., full width at half maximum (FWHM) and relative area under each component peak. It was assumed that the peaks were composed of several contributions corresponding to Al, N, C and O with different chemical states. Fig. 6a and b show the XPS spectra for the corresponding Al $2p_{3/2}$ and N 1s core levels of sample S(B). The major contribution in Fig. 6a, centered at 73.5 eV, is assigned to Al $2p_{3/2}$ in Al–N bonds. These values fall inside of a wide range of reported values for this transition, including 73.1 eV [24], 73.9 eV [25] and 74.7 eV [26–28]. The lower BE contribution at 72.8 eV, is accredited to metallic Al, in agreement (72.8–72.9 eV) with most reports [26,27,29], while the higher BE contribution at 74.7 eV is assigned to aluminium in oxide-like bonding, falling in the range of a variety of reported binding energies (74.4–74.8 eV) [24–26,29,30]. The heat treatment at 200 °C in vacuum did not significantly modify the surface, relative to the aluminium binding components, as demonstrated by the small differences between the values of the BE, FWHM and relative area under the peak of the Al $2p_{3/2}$ related components before and after heat treatment. This is indicated in Table 2. The major contribution of the N 1s core level, in Fig. 6b, of the same S(B) sample, centered at 397.2 eV, is assigned to N–Al bonding since it appears within the literature reported values and is considered to have a spread of approximately 0.4 eV [24,26,27]. Whereas, the two contributions at higher binding energies, centered at 398.5 and 399.5 eV, are assigned to N–C bonding, which in the form of triple and double bonds, as nitrile and imide groups, have been reported in a wide range of BEs covering our results [27,31–33]. The O 1s core level spectrum presents a major peak at 531.6 eV, characteristic of Al–O bonding in Al_2O_3, very close to that given in several reports [29,34–36]. Another component of the O 1s transition of minor intensity, at 534.5 eV, may be associated to physically adsorbed [26] molecular H_2O. The C 1s core level peak shows a major contribution centered at 284.5 eV, which was assigned to C–C bonding or adventitious carbon [27,33]. The curve fitting resulted in three other components of minor intensity at 283.5, 286.5 and 288.5 eV. These last three components may be associated to C in carbidic state [37], to C–N bonding [33] and to C–O bonding [27], respectively.

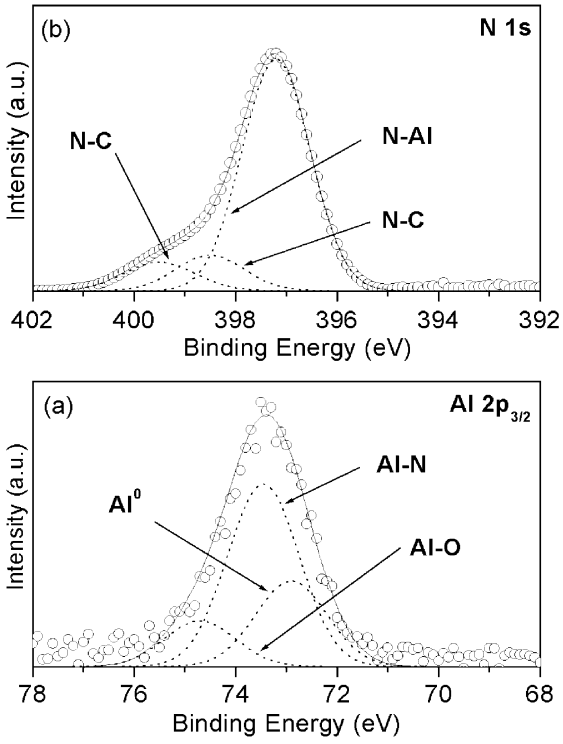

Fig. 6. The XPS spectra of sample S(B) for (a) Al $2p_{3/2}$ and (b) N 1s.

4. Discussion

It is observed that the optical and surface properties have a strong dependence on the deposition rate. The

Table 2
The BE, FWHM and relative area under the peaks of Al $2p_{3/2}$ and N 1s related components, before and after heat treatment

Core level	Peak assignment	Before heat treatment			After heat treatment		
		BE (eV)	FWHM (eV)	Area (%)	BE (eV)	FWHM (eV)	Area (%)
Al $2p_{3/2}$	Al metallic	72.8	1.0	27	72.6	1.1	27
	Al–N	73.5	1.0	58	73.3	1.0	61
	Al–O	74.7	1.0	15	74.8	1.0	12
N 1s	N nitride	397.2	1.0	78	397.4	1.0	78
	N–C (nitrile group)	398.5	1.0	12	398.5	1.0	15
	N–C (imine group)	399.5	1.0	10	399.5	1.0	7

films prepared using different deposition conditions are clearly separated into two groups in the refractive index (n) vs. photon energy graphs, one corresponding to the plasma current $I_p = 0.45$ A (high n) and the other to 0.2 A (low n). This probably indicates the importance of ion bombardment during the growth of this material since, for these stoichiometric films, it can be assumed that the value of the refractive index is directly related to the film density.

The XPS measurements reinforce the ellipsometer model since both techniques reveal the presence of Al_2O_3, Al and Al–N bonding at the near surface region. There is oxygen in the external layers of the films, even though the deposits were cooled down to less than 100 °C before being exposed to atmosphere. During the oxide formation on the surface it appears that the oxygen replaces the nitrogen atoms originally bonded to Al causing the formation of the oxide and the accumulation of Al on the surface. In these terms, our results are in agreement with the previously reported studies, showing that once the deposit is exposed to air, the outer surface of the AlN oxidizes, forming Al_2O_3, until equilibrium is reached when the oxide layer seals or passivates the AlN material. The RBS results also corroborate the observed elemental analysis and the presence of N–C bonding is expected given the presence of carbon contamination observed by the application of both surface and bulk techniques. It is interesting to note that there is little change in the relative concentrations of the detected elements on the surface of the AlN films before and after the heat treatment at 200°C indicating the stability at this temperature.

We have observed that the thickness of the oxide layer is reduced when higher plasma current and lower nitrogen concentration are used. This is probably a result of increased ion bombardment of the growing film, giving rise to a deposit with a considerably increased density or improved morphology. This idea is also supported by ellipsometric results, where a 5–10 nm thick layer of composite material ($Al_2O_3 + AlN$) is required to give good curve fitting for higher plasma current conditions, while the thickness of the composite surface layer had to be increased to 20–30 nm for good curve fitting when the plasma current is lower and/or the nitrogen concentration is higher.

There is a wide range of reported FTIR peak position of the $A_1(TO)$ mode for AlN from 660 to 675 cm^{-1} [38,39]. In our films, this peak appears near 673 cm^{-1}. This value is probably associated to some residual stress. Furthermore, the absence of Al–O absorption peak at approximately 460 cm^{-1} shows that the main bonding in our films is Al–N.

5. Conclusions

From the set of AlN thin films prepared by DC-reactive magnetron sputtering varying deposition parameters and analyzed by spectroscopic ellipsometry, XPS, RBS, XRD, SEM, AFM and FTIR, the following conclusions can be obtained.

The optical and surface properties have a strong dependence on the deposition rate. All prepared films present a composition close to AlN stoichiometry, even for nitrogen to argon gas concentrations below 1:2. The near surface of AlN films exposed to atmosphere is primarily composed of Al_2O_3 and the bulk is AlN with some minor contamination of oxygen and carbon. The thickness of the oxide layer is reduced when higher plasma current and lower nitrogen concentration are used. Deposits prepared at 400 °C present the best refractive index and deposition rate, for both utilized plasma currents.

Acknowledgments

The authors would like to gratefully thank J.A. Díaz, E. Aparicio, and J.A. Peralta for technical assistance.

References

[1] D. Brunner, H. Angerer, E. Bustarret, et al., J. Appl. Phys. 82 (1997) 5090.
[2] A. Mahmood, N. Rakov, M. Xiao, Mater. Lett., in press.
[3] M.N. Yoder, IEEE Trans. Electron Devices 43 (1996) 1633.
[4] J.S. Huang, X. Dong, X.D. Luo, et al., J. Crystal Growth 247 (2003) 84.
[5] J.L. Dupuie, E. Gulari, J. Vac. Sci. Technol. A 10 (1992) 18.
[6] Y. Huttel, H. Gomez, A. Cebollada, G. Armelles, M.I. Alonso, J. Crystal Growth 242 (2002) 116.
[7] R. Bensalem, A. Abid, B.J. Selly, Thin Solid Films 143 (1986) 141.
[8] H.-U. Baier, W. Moench, Appl. Surf. Sci. 56–58 (1992) 766.
[9] Z. Sitar, L.L. Smith, R.F. Davis, J. Crystal Growth 141 (1994) 11.
[10] S. Six, B. Rauschenbach, Thin Solid Films 415 (2002) 285.
[11] X. Li, T.L. Tansley, J. Appl. Phys. 68 (1990) 5369.
[12] W. Zhang, Y. Someno, M. Sasaki, T. Hirai, J. Crystal Growth 130 (1993) 308.
[13] C.R. Aardahl, J.W. Rogers Jr., H.K. Yun, Y. Ono, D.C. Tweet, S.-T. Hsu, Thin Solid Films 346 (1999) 174.
[14] V.A. Lavrenko, J. Desmaison, A.D. Panasyuk, M. Desmaison-Brut, J. Eur. Ceram. Soc. 23 (2003) 357.
[15] G.A. Slack, L.J. Schowalter, D. Morelli, J.A. Freitas Jr., J. Crystal Growth 246 (2002) 287.
[16] F. Ansart, H. Ganda, R. Saporte, J.P. Traverse, Thin Solid Films 260 (1995) 38.
[17] E. Andrade, Nucl. Instr. Meth. Phys. Res. B 57 (1991) 802.
[18] M. Mayer, SIMNRA User's Guide. Technical Report IPP 9/113, Max Plank Institut fur Plasmaphysik, Garching, Germany.
[19] R.F. Bunsha, Deposition Technologies for Films and Coatings, Noyes, Norwich, USA, 1982, p. 214.
[20] S. Loughin, R.H. French, in: (Ed.), Handbook of Optical Constants of Solids III, Academic Press, 1998, p. 373.
[21] H.Y. Joo, H.J. Kim, S.J. Kim, S.Y. Kim, Thin Solid Films 368 (2000) 67.
[22] M. Gadenne, J. Plon, P. Gaddene, Thin Solid Films 333 (1998) 251.
[23] H.-Y. Joo, H.J. Kim, S.J. Kim, S.Y. Kim, J. Vac. Sci. Technol. A 17 (1999) 862.

[24] D. Manova, V. Dimitrova, W. Fukarek, D. Karpuzov, Surf. Coat. Technol. 106 (1998) 205.
[25] J.A. Taylor, J.W. Rabalais, J. Chem. Phys. 75 (1981) 1735.
[26] S. Schoser, G. Brauchle, J. Forget, et al., Surf. Coat. Technol. 103 (1998) 222.
[27] J.F. Moulder, W.F. Stickle, P.E. Sobol, K.D. Bomben, Handbook of X-Ray Photoelectron Spectroscopy, Perkin-Elmer Corporation, Eden Prairie, USA, 1992.
[28] J. Huang, L. Wang, Q. Shen, C. Lin, M. Ostling, Thin Solid Films 340 (1999) 137.
[29] N. Laidani, L. Vanzetti, M. Anderle, A. Basillais, C. Boulmer-Leborgne, J. Perriere, Surf. Coat. Technol. 122 (1999) 242.
[30] N. Duez, B. Mutel, O. Dessaus, P. Goundman, J. Grimblot, Surf. Coat. Technol. 125 (2000) 79.
[31] F. Rossi, B. Andre, A. van Vin, et al., Thin Solid Films 253 (1994) 118.
[32] F. Weich, J. Widany, Th. Frauenheim, Phys. Rev. Lett. 78 (1997) 3326.
[33] G. Soto, E.C. Samano, R. Machorro, M.H. Farias, L. Cota-Araiza, Appl. Surf. Sci. 183 (2001) 246.
[34] C.D. Wagner, D.E. Passoja, H.F. Hillery, et al., J. Vac. Sci. Technol. 21 (1982) 933.
[35] V.I. Nefedov, D. Gati, B.F. Dzhurinskii, N.P. Sergushin, Y.V. Saljn, Zh. Neorg. Khim. 20 (1975) 2307.
[36] M. Takagi-Kawai, M. Soma, T. Onishi, K. Tamaru, Can. J. Chem. 58 (1980) 2132.
[37] P. Stoyanov, S. Akhter, J.M. White, Surf. Interface Anal. 15 (1990) 509.
[38] G. Fernández-Catá, G. Rojas-Lorenzo, J.A. Odriozola, L.J. Alvarez, Chem. Phys. Lett. 356 (2002) 127.
[39] C.T.M. Ribeiro, A.R. Zanata, F. Alvarez, J. Non-Cryst. Sol. 299–302 (2002) 323.